Commun. Comput. Phys.
doi: 10.4208/cicp.180513.230514a

Vol. **16**, No. 5, pp. 1323-1354
November 2014

Solving Two-Mode Shallow Water Equations Using Finite Volume Methods

Manuel Jesús Castro Díaz[1,*], Yuanzhen Cheng[2], Alina Chertock[3] and Alexander Kurganov[2]

[1] *Dpto. de Análisis Matemático, Facultad de Ciencias, Universidad de Málaga, Campus de Teatinos, 29071 Málaga, Spain.*
[2] *Mathematics Department, Tulane University, New Orleans, LA 70118, USA.*
[3] *Department of Mathematics, North Carolina State University, Raleigh, NC 27695, USA.*

Received 18 May 2013; Accepted (in revised version) 23 May 2014

Communicated by Chi-Wang Shu

Available online 29 August 2014

Abstract. In this paper, we develop and study numerical methods for the two-mode shallow water equations recently proposed in [S. STECHMANN, A. MAJDA, and B. KHOUIDER, Theor. Comput. Fluid Dynamics, 22 (2008), pp. 407–432]. Designing a reliable numerical method for this system is a challenging task due to its conditional hyperbolicity and the presence of nonconservative terms. We present several numerical approaches—two operator splitting methods (based on either Roe-type upwind or central-upwind scheme), a central-upwind scheme and a path-conservative central-upwind scheme—and test their performance in a number of numerical experiments. The obtained results demonstrate that a careful numerical treatment of nonconservative terms is crucial for designing a robust and highly accurate numerical method.

AMS subject classifications: 76M12, 65M08, 86-08, 86A10, 35L65, 35L67

Key words: Two-mode shallow water equations, nonconservative products, conditional hyperbolicity, finite volume methods, central-upwind schemes, splitting methods, upwind schemes.

1 Introduction

The goal of this paper is to develop an accurate, efficient and robust numerical method for the two-mode shallow water equations (2MSWE):

*Corresponding author. *Email addresses:* castro@anamat.cie.uma.es (M. J. Castro Díaz), ycheng5@tulane.edu (Y. Cheng), chertock@math.ncsu.edu (A. Chertock), kurganov@math.tulane.edu (A. Kurganov)

$$\begin{cases} \dfrac{\partial u_1}{\partial t}-\dfrac{\partial \theta_1}{\partial x}=-\dfrac{3}{\sqrt{2}}\left[u_2\dfrac{\partial u_1}{\partial x}+\dfrac{1}{2}u_1\dfrac{\partial u_2}{\partial x}\right], \\ \dfrac{\partial \theta_1}{\partial t}-\dfrac{\partial u_1}{\partial x}=-\dfrac{1}{\sqrt{2}}\left[2u_1\dfrac{\partial \theta_2}{\partial x}-u_2\dfrac{\partial \theta_1}{\partial x}+4\theta_2\dfrac{\partial u_1}{\partial x}-\dfrac{1}{2}\theta_1\dfrac{\partial u_2}{\partial x}\right], \\ \dfrac{\partial u_2}{\partial t}-\dfrac{\partial \theta_2}{\partial x}=0, \\ \dfrac{\partial \theta_2}{\partial t}-\dfrac{1}{4}\dfrac{\partial u_2}{\partial x}=-\dfrac{1}{2\sqrt{2}}\left[u_1\dfrac{\partial \theta_1}{\partial x}-\theta_1\dfrac{\partial u_1}{\partial x}\right], \end{cases} \tag{I}$$

which can also be written in the following vector form:

$$\boldsymbol{U}_t+\boldsymbol{F}_{\mathbf{I}}(\boldsymbol{U})_x=B_{\mathbf{I}}(\boldsymbol{U})\boldsymbol{U}_x, \tag{1.1}$$

where

$$\boldsymbol{U}=\begin{pmatrix} u_1 \\ \theta_1 \\ u_2 \\ \theta_2 \end{pmatrix}, \quad \boldsymbol{F}_{\mathbf{I}}(\boldsymbol{U})=\begin{pmatrix} -\theta_1 \\ -u_1 \\ -\theta_2 \\ -\dfrac{1}{4}u_2 \end{pmatrix}, \quad B_{\mathbf{I}}(\boldsymbol{U})=\begin{pmatrix} -\dfrac{3}{\sqrt{2}}u_2 & 0 & -\dfrac{3}{2\sqrt{2}}u_1 & 0 \\ -2\sqrt{2}\theta_2 & \dfrac{1}{\sqrt{2}}u_2 & \dfrac{1}{2\sqrt{2}}\theta_1 & -\sqrt{2}u_1 \\ 0 & 0 & 0 & 0 \\ \dfrac{1}{2\sqrt{2}}\theta_1 & -\dfrac{1}{2\sqrt{2}}u_1 & 0 & 0 \end{pmatrix}.$$

Here, $u_1(x,t)$,$u_2(x,t)$ and $\theta_1(x,t)$,$\theta_2(x,t)$ are the first two baroclinic modes of the vertical expansions of the velocity and potential temperature, respectively.

The system (1.1) has been derived in [36] as a simplified model that describes nonlinear dynamics of waves with different vertical profiles. Compared to the two-layer shallow water equations studied, for example, in [1,4–6,9,23,26,39], the 2MSWE have several important differences and similarities, both physical and mathematical. The two-layer shallow water equations describe flows with two layers of different densities that have no horizontal variations within each layer, and thus no thermodynamic processes are included in this model. In contrast, the 2MSWE include thermodynamic effects through the potential temperatures θ_1 and θ_2. In addition, while the two-layer shallow water equations assume a free upper surface, the 2MSWE are based on a rigid upper lid approximation. Also, the vertical structure of the flow in the two-layer shallow water equations consists of the barotropic and first baroclinic modes, while in the 2MSWE both the first and second baroclinic modes are taken into account. From the mathematical point of view, the two-layer shallow water equations and 2MSWE have a lot in common: Both are systems of nonconservative PDEs, both conserve energy, both are conditionally hyperbolic only, and both have eigenstructures that are analytically intractable.

The presence of nonconservative terms $B_{\mathbf{I}}(\boldsymbol{U})\boldsymbol{U}_x$ in (1.1) makes both the theoretical analysis and development of numerical methods for the system (**I**) a very difficult task. In fact, when the solutions are discontinuous, which is a common feature of nonlinear hyperbolic systems, these nonconservative terms are not well defined in the distributional

framework and the usual concept of weak solution cannot be used. Instead they should be understood as the Borel measures as it was done in [13].

A first numerical method for the nonconservative 2MSWE was developed in [36]. The main idea of the approach proposed in [36] was to split the equations into conservative and nonconservative parts and to solve each part with an appropriate method. Namely, in [36], the system (**I**) was rewritten as

$$\begin{cases} \dfrac{\partial u_1}{\partial t}+\dfrac{\partial}{\partial x}\left[-\theta_1+\dfrac{3}{\sqrt{2}}u_1u_2\right]=\dfrac{3}{2\sqrt{2}}u_1\dfrac{\partial u_2}{\partial x}, \\ \dfrac{\partial \theta_1}{\partial t}+\dfrac{\partial}{\partial x}\left[-u_1+\sqrt{2}u_1\theta_2-\dfrac{1}{\sqrt{2}}u_2\theta_1\right]=-\dfrac{1}{\sqrt{2}}\left[2\theta_2\dfrac{\partial u_1}{\partial x}+\dfrac{1}{2}\theta_1\dfrac{\partial u_2}{\partial x}\right], \\ \dfrac{\partial u_2}{\partial t}+\dfrac{\partial}{\partial x}[-\theta_2]=0, \\ \dfrac{\partial \theta_2}{\partial t}+\dfrac{\partial}{\partial x}\left[-\dfrac{1}{4}u_2\right]=-\dfrac{1}{2\sqrt{2}}\left[u_1\dfrac{\partial \theta_1}{\partial x}-\theta_1\dfrac{\partial u_1}{\partial x}\right], \end{cases} \tag{**II**}$$

or in a vector form similar to (1.1):

$$\boldsymbol{U}_t+\boldsymbol{F}_{\mathbf{II}}(\boldsymbol{U})_x=B_{\mathbf{II}}(\boldsymbol{U})\boldsymbol{U}_x, \tag{1.2}$$

with

$$\boldsymbol{F}_{\mathbf{II}}(\boldsymbol{U})=\begin{pmatrix} -\theta_1+\dfrac{3}{\sqrt{2}}u_1u_2 \\ -u_1+\sqrt{2}u_1\theta_2-\dfrac{1}{\sqrt{2}}u_2\theta_1 \\ -\theta_2 \\ -\dfrac{1}{4}u_2 \end{pmatrix}, \quad B_{\mathbf{II}}(\boldsymbol{U})=\begin{pmatrix} 0 & 0 & \dfrac{3}{2\sqrt{2}}u_1 & 0 \\ -\sqrt{2}\theta_2 & 0 & -\dfrac{1}{2\sqrt{2}}\theta_1 & 0 \\ 0 & 0 & 0 & 0 \\ \dfrac{1}{2\sqrt{2}}\theta_1 & -\dfrac{1}{2\sqrt{2}}u_1 & 0 & 0 \end{pmatrix}.$$

Then, using the Strang operator splitting [37], the hyperbolic system of conservation laws,

$$\boldsymbol{U}_t+\boldsymbol{F}_{\mathbf{II}}(\boldsymbol{U})_x=\boldsymbol{0}, \tag{1.3}$$

was solved using the Nessyahu-Tadmor scheme [30], while the nonconservative system,

$$\boldsymbol{U}_t=B_{\mathbf{II}}(\boldsymbol{U})\boldsymbol{U}_x, \tag{1.4}$$

was integrated using a straightforward semi-discrete approach. The method produced good results for problems presented in [36]. It is well known, however, that a special treatment of nonconservative terms is required since the computed solution heavily depends on the way the nonconservative terms are discretized [2,7,8,10,28,29,31,33].

In the past few years, many numerical methods for systems with nonconservative forms have been proposed, see, e.g., [1,4–10,12,26,28,31,32]. One of the ways to overcome the difficulty related to the presence of such terms in the two-layer shallow water

model is to use the splitting between the upper and lower layers as it was done in [4,5]. According to [4], the equations for each layer are solved separately, which simplifies the eigenstructure of the problem and allows one to easily apply upwinding. However, the method proposed in [4] suffers from the lack of total momentum conservation, which may lead to the convergence of the computed solution towards unphysical states. A more systematic approach was advocated in [7, 8, 10, 12, 28, 29, 29, 31–33], where path-conservative numerical schemes have been developed. These schemes rely on the rigorous definition of the weak solution, which depends on the choice of a family of paths in the phase space.

A simpler approach was introduced in [23] where the two-layer system was rewritten in such a way that the magnitude of nonconservative terms became small in all practical situations (when the magnitude of surface waves is much smaller than the magnitude of internal waves). The resulting system was then solved using a second-order central-upwind scheme [19–21, 24]. The approach proposed in [23] clearly reduces the dependence of numerical methods from the discretization of the nonconservative terms, but still may fail in examples in which the surface waves are not small.

Central-upwind schemes are Riemann-problem-solver-free Godunov-type methods that were originally introduced for general hyperbolic systems of conservation laws in [19, 20, 24] and extended to a variety of shallow water models [18, 21, 22]. They admit a simple semi-discrete form (see Section 2) and can be also applied quite easily to both the systems (**I**) and (**II**), in which case there is no need to split between the conservative and nonconservative parts of the system, so splitting errors can be avoided. However, as it was mentioned above, if the nonconservative terms in the systems (**I**) and (**II**) are not small, one may expect the central-upwind scheme to fail in certain examples. Indeed, our numerical experiments reported in Section 5 clearly demonstrate that the solutions obtained by a straightforward application of the central-upwind schemes heavily depend on the way the nonconservative 2MSWE are written, which makes the schemes non-robust, in the sense that it may fail to capture a physically relevant solution.

In this paper, we mainly study two numerical methods for solving the nonconservative 2MSWE. We first consider a different way of operator splitting. To this end, we rewrite the system (**I**) as

$$\begin{cases} \dfrac{\partial u_1}{\partial t}+\dfrac{\partial}{\partial x}\left[\dfrac{3}{\sqrt{2}}u_1u_2-\theta_1\right]=\dfrac{3}{2\sqrt{2}}u_1\dfrac{\partial u_2}{\partial x}, \\ \dfrac{\partial \theta_1}{\partial t}+\dfrac{\partial}{\partial x}\left[-u_1+2\sqrt{2}u_1\theta_2-\dfrac{1}{\sqrt{2}}\theta_1u_2\right]=\sqrt{2}u_1\dfrac{\partial \theta_2}{\partial x}-\dfrac{1}{2\sqrt{2}}\theta_1\dfrac{\partial u_2}{\partial x}, \\ \dfrac{\partial u_2}{\partial t}+\dfrac{\partial}{\partial x}[-\theta_2]=0, \\ \dfrac{\partial \theta_2}{\partial t}+\dfrac{\partial}{\partial x}\left[-\dfrac{1}{4}u_2\right]=\dfrac{1}{2\sqrt{2}}\theta_1\dfrac{\partial u_1}{\partial x}-\dfrac{1}{2\sqrt{2}}u_1\dfrac{\partial \theta_1}{\partial x}. \end{cases} \tag{**III**}$$

The system (**III**) can be written in the following vector form:

$$\begin{cases} (\boldsymbol{U}_1)_t+\boldsymbol{F}_1(\boldsymbol{U})_x=B_1(\boldsymbol{U}_1)(\boldsymbol{U}_2)_x, & (1.5a)\\ (\boldsymbol{U}_2)_t+\boldsymbol{F}_2(\boldsymbol{U}_2)_x=B_2(\boldsymbol{U}_1)(\boldsymbol{U}_1)_x, & (1.5b)\end{cases}$$

where

$$\boldsymbol{U}_1=\begin{pmatrix}u_1\\ \theta_1\end{pmatrix},\quad \boldsymbol{F}_1(\boldsymbol{U})=\begin{pmatrix}\frac{3}{\sqrt{2}}u_1u_2-\theta_1\\ -u_1+2\sqrt{2}u_1\theta_2-\frac{1}{\sqrt{2}}\theta_1u_2\end{pmatrix},\quad B_1(\boldsymbol{U}_1)=\begin{pmatrix}\frac{3}{2\sqrt{2}}u_1 & 0\\ -\frac{1}{2\sqrt{2}}\theta_1 & \sqrt{2}u_1\end{pmatrix}, \tag{1.6}$$

and

$$\boldsymbol{U}_2=\begin{pmatrix}u_2,\\ \theta_2\end{pmatrix},\quad \boldsymbol{F}_2(\boldsymbol{U}_2)=\begin{pmatrix}-\theta_2\\ 1\\ -\frac{1}{4}u_2\end{pmatrix},\quad B_2(\boldsymbol{U}_1)=\begin{pmatrix}0 & 0\\ \frac{1}{2\sqrt{2}}\theta_1 & -\frac{1}{2\sqrt{2}}u_1\end{pmatrix}. \tag{1.7}$$

This way one can split between the first and second modes and solve the systems (1.5a) and (1.5b) separately as we demonstrate in Section 3. Such a splitting approach is advantageous since the right-hand side (RHS) of (1.5a) contains only $(\boldsymbol{U}_2)_x$, while the RHS of (1.5b) contains only $(\boldsymbol{U}_1)_x$, which are considered to be given functions at the corresponding splitting steps. Moreover, the systems (1.5a) and (1.5b) are linear systems (with variable coefficients) and thus can be easily solved using the upwind approach as it is described in Section 3.

The designed splitting method performs very well in many applications, but still fails in some examples (see Section 5), which suggests that splitting between the modes is probably insufficient to design a robust numerical method for the 2MSWE.

Another direction we explore in an attempt to design a robust and highly accurate numerical method for 2MSWE is based on a path-conservative central-upwind scheme, which was recently proposed in the context of two-layer shallow water equations, [11]. As it has been demonstrated in [11], if the linear path is considered, the results obtained by the path-conservative central-upwind scheme are independent of the form in which the system is written. Details on the application of the path-conservative central-upwind scheme to the systems (**I**), (**II**) and (**III**) are provided in Section 4. Our numerical experiments, reported in Section 5, confirm that the path-conservative central-upwind scheme both provides a high-resolution of the computed solution and is capable to accurately and robustly treat nonconservative terms appearing in 2MSWE.

2 Finite volume method setting

In this section, we briefly describe a general framework of semi-discrete finite volume methods, which will serve as a basis for the derivation of the splitting method and path-conservative central-upwind scheme below. To this extent, we consider a system

$$\boldsymbol{U}_t+\boldsymbol{F}(\boldsymbol{U})_x=\boldsymbol{R}(\boldsymbol{U},\boldsymbol{U}_x), \tag{2.1}$$

and, for simplicity, introduce a uniform spatial grid $x_\alpha := \alpha\Delta x$, where Δx is a small spatial scale and α is any spatial index, either integer or half-integer. We denote by I_j the finite volume cells $I_j := [x_{j-\frac{1}{2}}, x_{j+\frac{1}{2}}]$ and by $\overline{\boldsymbol{U}}_j(t)$ and $\overline{\boldsymbol{R}}_j(t)$ the cell averages,

$$\overline{\boldsymbol{U}}_j(t) \approx \frac{1}{\Delta x}\int_{I_j} \boldsymbol{U}(x,t)dx, \quad \overline{\boldsymbol{R}}_j(t) \approx \frac{1}{\Delta x}\int_{I_j} \boldsymbol{R}(\boldsymbol{U},\boldsymbol{U}_x)dx,$$

of the computed solution **U** and source term **R**, respectively. A semi-discretization of (2.1) is the following system of ODEs:

$$\frac{d}{dt}\overline{\boldsymbol{U}}_j(t) = -\frac{\boldsymbol{H}_{j+\frac{1}{2}}(t) - \boldsymbol{H}_{j-\frac{1}{2}}(t)}{\Delta x} + \overline{\boldsymbol{R}}_j(t), \tag{2.2}$$

which should be numerically integrated by an appropriate ODE solver. Note that the quantities $\overline{\boldsymbol{U}}_j$, $\overline{\boldsymbol{R}}_j$ and $\boldsymbol{H}_{j+\frac{1}{2}}$ depend on t, but we will suppress this dependence throughout the paper for brevity.

In the system (2.2), $\boldsymbol{H}_{j+\frac{1}{2}}$ are numerical fluxes, which are to be derived in order to complete the description of the semi-discrete finite-volume method. In Section 3 and Section 4, we provide the reader with a detailed derivation of the numerical fluxes for the proposed splitting method and path-conservative central-upwind scheme, respectively. A common feature in the derivations below is that the numerical fluxes are computed from a piecewise polynomial reconstruction of $\boldsymbol{U}$, which we denote by $\widetilde{\boldsymbol{U}}(x)$, i.e., $\boldsymbol{H}_{j+\frac{1}{2}} = \mathcal{H}(\widetilde{\boldsymbol{U}})$, where $\mathcal{H}$ is a given function. To design a second-order scheme, we use conservative piecewise linear reconstructions of form

$$\widetilde{\boldsymbol{U}}(x) := \overline{\boldsymbol{U}}_j + (\boldsymbol{U}_x)_j(x - x_j), \quad x_{j-\frac{1}{2}} < x < x_{j+\frac{1}{2}}. \tag{2.3}$$

Here, the numerical derivatives $(\boldsymbol{U}_x)_j$ are to be at least first-order approximations of $\boldsymbol{U}_x(x_j,t)$, computed using a nonlinear limiter needed to ensure a non-oscillatory nature of the reconstruction (2.3). In our numerical experiments, we have used the generalized minmod limiter (see, e.g., [30, 38, 40]):

$$(\mathbf{U}_x)_j = \text{minmod}\left(\gamma\frac{\overline{\boldsymbol{U}}_j - \overline{\boldsymbol{U}}_{j-1}}{\Delta x}, \frac{\overline{\boldsymbol{U}}_{j+1} - \overline{\boldsymbol{U}}_{j-1}}{2\Delta x}, \gamma\frac{\overline{\boldsymbol{U}}_{j+1} - \overline{\boldsymbol{U}}_j}{\Delta x}\right), \quad \gamma \in [1,2], \tag{2.4}$$

which can be applied in a componentwise manner to either characteristic (Section 3) or conservative (Section 4) variables. The minmod function is defined as:

$$\text{minmod}(z_1, z_2, \cdots) := \begin{cases} \min_j\{z_j\}, & \text{if } z_j > 0, \forall j, \\ \max_j\{z_j\}, & \text{if } z_j < 0, \forall j, \\ 0, & \text{otherwise,} \end{cases}$$

and the parameter γ can be used to control the amount of numerical viscosity present in the resulting scheme. We recall that larger values of γ correspond to less dissipative but, in general, more oscillatory reconstructions, see [25, 30].

In what follows, we first present finite-volume methods for the system (**III**), which are implemented in conjunction with a splitting approach (see Section 3) and then, in Section 4, describe a path-conservative central-upwind scheme for the systems (**I**), (**II**), and (**III**).

3 Splitting method

Consider the system (**III**), and denote by $\mathcal{L}_1$ the exact solution operator associated with the first sub-system (1.5a) (assuming that $\boldsymbol{U}_2$ is fixed) and by $\mathcal{L}_2$ the exact solution operator associated with the second sub-system (1.5b) (assuming that $\boldsymbol{U}_1$ is fixed).

Suppose that the solution of the system (**III**) is available at time t. We then introduce a (small) time step Δt and evolve the solution from t to $t+\Delta t$ in three sub-steps according to the second-order Strang splitting:

$$\boldsymbol{U}(x,t+\Delta t)=\mathcal{L}_1(\Delta t/2)\mathcal{L}_2(\Delta t)\mathcal{L}_1(\Delta t/2)\boldsymbol{U}(x,t),$$

where

$$\boldsymbol{U}=\begin{pmatrix}\boldsymbol{U}_1\\ \boldsymbol{U}_2\end{pmatrix}.$$

To design a splitting based numerical method, the exact solution operators $\mathcal{L}_1$ and $\mathcal{L}_2$ have to be replaced with the approximate ones and the numerical schemes for (1.5a) and (1.5b) have to be derived.

3.1 Upwind scheme for (1.5a)

We begin with the numerical solution of the first sub-system (1.5a), which is approximated using the Roe-type upwind scheme. To this end, we first note that (1.5a) can be rewritten in the following quasilinear form:

$$(\boldsymbol{U}_1)_t+A_1(\boldsymbol{U}_2)(\boldsymbol{U}_1)_x=\boldsymbol{R}_1(\boldsymbol{U}_1,(\boldsymbol{U}_2)_x), \tag{3.1}$$

where

$$A_1(\boldsymbol{U}_2):=\frac{\partial \boldsymbol{F}_1}{\partial \boldsymbol{U}_1}=\begin{pmatrix}\frac{3}{\sqrt{2}}u_2 & -1\\ 2\sqrt{2}\theta_2-1 & -\frac{1}{\sqrt{2}}u_2\end{pmatrix},\quad \boldsymbol{R}_1=B_1(\boldsymbol{U}_1)(\boldsymbol{U}_2)_x, \tag{3.2}$$

and $\boldsymbol{F}_1(\boldsymbol{U})$ and $B_1(\boldsymbol{U}_1)$ are defined in (1.6). As one can clearly see from (3.1) and (3.2), the system (1.5a) is a linear system with variable coefficients (since $\boldsymbol{U}_2$ is now assumed to be fixed).

According to the finite volume framework outlined in Section 2, $\boldsymbol{U}_1$ is evolved in time by solving the following ODE system:

$$\frac{d}{dt}(\overline{\boldsymbol{U}}_1)_j=-\frac{(\boldsymbol{H}_1)_{j+\frac{1}{2}}-(\boldsymbol{H}_1)_{j-\frac{1}{2}}}{\Delta x}+(\overline{\boldsymbol{R}}_1)_j,$$

where $(\boldsymbol{H}_1)_{j+\frac{1}{2}}$ is an upwind approximation of the flux $\boldsymbol{F}_1(\boldsymbol{U})$ at point $x=x_{j+\frac{1}{2}}$. To derive this approximation, we freeze the coefficients of A_1 and diagonalize $A_1((\boldsymbol{U}_2)_{j+\frac{1}{2}})$ using the matrix

$$(Q_1)_{j+\frac{1}{2}}$$
$$=\begin{pmatrix} \sqrt{2}(u_2)_{j+\frac{1}{2}}-\sqrt{1+2(u_2)^2_{j+\frac{1}{2}}-2\sqrt{2}(\theta_2)_{j+\frac{1}{2}}} & \sqrt{2}(u_2)_{j+\frac{1}{2}}+\sqrt{1+2(u_2)^2_{j+\frac{1}{2}}-2\sqrt{2}(\theta_2)_{j+\frac{1}{2}}} \\ 2\sqrt{2}(\theta_2)_{j+\frac{1}{2}}-1 & 2\sqrt{2}(\theta_2)_{j+\frac{1}{2}}-1 \end{pmatrix}.$$

Here, $(u_2)_{j+\frac{1}{2}}$ and $(\theta_2)_{j+\frac{1}{2}}$ are the upwinded values of u_2 and θ_2 at $x=x_{j+\frac{1}{2}}$, respectively (these values are assumed to be computed and frozen at the end of the preceding splitting step). Thus, we obtain

$$(\Lambda_1)_{j+\frac{1}{2}}=:\begin{pmatrix} (\lambda_1)^-_{j+\frac{1}{2}} & 0 \\ 0 & (\lambda_1)^+_{j+\frac{1}{2}} \end{pmatrix}=(Q_1^{-1})_{j+\frac{1}{2}}(A_1)_{j+\frac{1}{2}}(Q_1)_{j+\frac{1}{2}}$$
$$=\begin{pmatrix} \frac{1}{\sqrt{2}}(u_2)_{j+\frac{1}{2}}-\sqrt{1+2(u_2)^2_{j+\frac{1}{2}}-2\sqrt{2}(\theta_2)_{j+\frac{1}{2}}} & 0 \\ 0 & \frac{1}{\sqrt{2}}(u_2)_{j+\frac{1}{2}}+\sqrt{1+2(u_2)^2_{j+\frac{1}{2}}-2\sqrt{2}(\theta_2)_{j+\frac{1}{2}}} \end{pmatrix}$$

and define a corresponding set of the characteristic variables

$$\boldsymbol{W}_1\equiv\begin{pmatrix}\hat{u}_1\\ \hat{\theta}_1\end{pmatrix}:=(Q_1^{-1})_{j+\frac{1}{2}}\boldsymbol{U}_1.$$

We emphasize that these variables only need to be computed locally (near $x=x_{j+\frac{1}{2}}$) to obtain the linear pieces in cells I_j and I_{j+1},

$$(\overline{\boldsymbol{W}}_1)_j+((\boldsymbol{W}_1)_x)_j(x-x_j),\quad (\overline{\boldsymbol{W}}_1)_{j+1}+((\boldsymbol{W}_1)_x)_{j+1}(x-x_{j+1}),$$

which are, in turn, used to evaluate the two one-sided point values at $x=x_{j+\frac{1}{2}}$:

$$(\boldsymbol{W}_1)^+_{j+\frac{1}{2}}=(\overline{\boldsymbol{W}}_1)_{j+1}-\frac{\Delta x}{2}((\boldsymbol{W}_1)_x)_{j+1},$$
$$(\boldsymbol{W}_1)^-_{j+\frac{1}{2}}=(\overline{\boldsymbol{W}}_1)_{j}+\frac{\Delta x}{2}((\boldsymbol{W}_1)_x)_{j}.$$

The upwinded values of u_1 and θ_1 at $x=x_{j+\frac{1}{2}}$ are then computed by

$$\begin{pmatrix}(u_1)_{j+\frac{1}{2}}\\ (\theta_1)_{j+\frac{1}{2}}\end{pmatrix}=(Q_1)_{j+\frac{1}{2}}\begin{pmatrix}(\hat{u}_1)^{\mp}_{j+\frac{1}{2}}\\ (\hat{\theta}_1)^{\mp}_{j+\frac{1}{2}}\end{pmatrix},$$

where the signs in the upper indices of $(\hat{u}_1)^{\mp}_{j+\frac{1}{2}}$ and $(\hat{\theta}_1)^{\mp}_{j+\frac{1}{2}}$ correspond to the signs of the eigenvalues $(\lambda_1)^{-}_{j+\frac{1}{2}}$ and $(\lambda_1)^{+}_{j+\frac{1}{2}}$, respectively. Using the obtained values of $(u_1)_{j+\frac{1}{2}}$ and $(\theta_1)_{j+\frac{1}{2}}$, we evaluate the numerical flux at $x=x_{j+\frac{1}{2}}$:

$$(\boldsymbol{H}_1)_{j+\frac{1}{2}}=\boldsymbol{F}_1\left((u_1)_{j+\frac{1}{2}},(\theta_1)_{j+\frac{1}{2}},(u_2)_{j+\frac{1}{2}},(\theta_2)_{j+\frac{1}{2}}\right),$$

and compute the numerical source term $(\overline{\boldsymbol{R}}_1)_j$ in the following manner:

$$(\overline{\boldsymbol{R}}_1)_j=\frac{1}{2\sqrt{2}\Delta x}\begin{pmatrix}3(\overline{u}_1)_j\left[(u_2)_{j+\frac{1}{2}}-(u_2)_{j-\frac{1}{2}}\right]\\ 4(\overline{u}_1)_j\left[(\theta_2)_{j+\frac{1}{2}}-(\theta_2)_{j-\frac{1}{2}}\right]-(\overline{\theta}_1)_j\left[(u_2)_{j+\frac{1}{2}}-(u_2)_{j-\frac{1}{2}}\right]\end{pmatrix}.$$

3.2 Upwind scheme for (1.5b)

We now consider the second sub-system (1.5b), which is rewritten as

$$(\boldsymbol{U}_2)_t+A_2(\boldsymbol{U}_2)_x=\boldsymbol{R}_2(\boldsymbol{U}_1,(\boldsymbol{U}_1)_x),$$

where

$$A_2:=\frac{\partial \boldsymbol{F}_2}{\partial \boldsymbol{U}_2}=\begin{pmatrix}0 & -1\\ -\frac{1}{4} & 0\end{pmatrix},\quad \boldsymbol{R}_2=B_2(\boldsymbol{U}_1)(\boldsymbol{U}_1)_x,$$

where $\boldsymbol{F}_2(\boldsymbol{U}_2)$ and $B_2(\boldsymbol{U}_1)$ are defined in (1.7). Following the finite volume approach described in Section 2, $\boldsymbol{U}_2$ is evolved in time by solving the system of ODEs:

$$\frac{d}{dt}(\overline{\boldsymbol{U}}_2)_j=-\frac{(\boldsymbol{H}_2)_{j+\frac{1}{2}}-(\boldsymbol{H}_2)_{j-\frac{1}{2}}}{\Delta x}+(\overline{\boldsymbol{R}}_2)_j,$$

where $(\boldsymbol{H}_2)_{j+\frac{1}{2}}$ is an upwind approximation of the flux $\boldsymbol{F}_2(\boldsymbol{U}_2)$ at $x=x_{j+\frac{1}{2}}$ derived as follows. First we diagonalize the matrix A_2:

$$\Lambda_2=Q_2^{-1}A_2Q_2=\begin{pmatrix}-\frac{1}{2} & 0\\ 0 & \frac{1}{2}\end{pmatrix}=:\begin{pmatrix}\lambda_2^- & 0\\ 0 & \lambda_2^+\end{pmatrix},\qquad Q_2=\begin{pmatrix}2 & -2\\ 1 & 1\end{pmatrix},$$

and define the characteristic variables

$$\boldsymbol{W}_2\equiv\begin{pmatrix}\hat{u}_2\\ \hat{\theta}_2\end{pmatrix}:=Q_2^{-1}\boldsymbol{U}_2,$$

that is,

$$\hat{u}_2:=\frac{1}{4}(2\theta_2+u_2),\quad \hat{\theta}_2=\frac{1}{4}(2\theta_2-u_2).$$

We then obtain a piecewise linear reconstruction in the characteristic space:

$$\widetilde{\boldsymbol{W}}_2(x):=(\overline{\boldsymbol{W}}_2)_j+((\boldsymbol{W}_2)_x)_j(x-x_j),\quad x_{j-\frac{1}{2}}<x<x_{j+\frac{1}{2}},\quad \forall j,$$

and compute the point values at $x=x_{j+\frac{1}{2}}$ by

$$(\boldsymbol{W}_2)^+_{j+\frac{1}{2}}=(\overline{\boldsymbol{W}}_2)_{j+1}-\frac{\Delta x}{2}((\boldsymbol{W}_2)_x)_{j+1},$$
$$(\boldsymbol{W}_2)^-_{j+\frac{1}{2}}=(\overline{\boldsymbol{W}}_2)_{j}+\frac{\Delta x}{2}((\boldsymbol{W}_2)_x)_{j}.$$

Since $\lambda_2^-<0<\lambda_2^+$, we use the corresponding one-sided values $(\hat{u}_2)^+_{j+\frac{1}{2}}$ and $(\hat{\theta}_2)^-_{j+\frac{1}{2}}$ to obtain the upwind flux

$$(\boldsymbol{H}_2)_{j+\frac{1}{2}}=\boldsymbol{F}_2\Big((u_2)_{j+\frac{1}{2}},(\theta_2)_{j+\frac{1}{2}}\Big),$$

where

$$\begin{pmatrix}(u_2)_{j+\frac{1}{2}}\\(\theta_2)_{j+\frac{1}{2}}\end{pmatrix}:=Q_2\begin{pmatrix}(\hat{u}_2)^+_{j+\frac{1}{2}}\\(\hat{\theta}_2)^-_{j+\frac{1}{2}}\end{pmatrix}=\begin{pmatrix}2(\hat{u}_2)^+_{j+\frac{1}{2}}-2(\hat{\theta}_2)^-_{j+\frac{1}{2}}\\(\hat{u}_2)^+_{j+\frac{1}{2}}+(\hat{\theta}_2)^-_{j+\frac{1}{2}}\end{pmatrix}.$$

The numerical source term $(\overline{\boldsymbol{R}}_2)_j$ is computed based on u_1 and θ_1, which are fixed and equal to

$$(\overline{\boldsymbol{R}}_2)_j=\frac{1}{2\sqrt{2}\Delta x}\begin{pmatrix}0\\(\overline{\theta}_1)_j\Big[(u_1)_{j+\frac{1}{2}}-(u_1)_{j-\frac{1}{2}}\Big]-(\overline{u}_1)_j\Big[(\theta_1)_{j+\frac{1}{2}}-(\theta_1)_{j-\frac{1}{2}}\Big]\end{pmatrix},$$

where $(u_1)_{j+\frac{1}{2}}$ and $(\theta_1)_{j+\frac{1}{2}}$ are the upwinded values of u_1 and θ_1 at $x=x_{j+\frac{1}{2}}$, which were obtained at the end of the previous splitting step described in Section 3.1.

4 Path-conservative central-upwind scheme

In this section, we design a robust and highly accurate numerical method for the 2MSWE, which is based on a recently proposed path-conservative central-upwind scheme [11]. For the sake of the reader, we begin the section with a brief description of a second-order central-upwind scheme from [20] and then develop its path-conservative version, which is applied to the systems (**I**), (**II**) and (**III**).

4.1 Central-upwind scheme for the 2MSWE

We consider the system (2.1) with $\boldsymbol{R}(\boldsymbol{U},\boldsymbol{U}_x)=B(\boldsymbol{U})\boldsymbol{U}_x$, that is,

$$\boldsymbol{U}_t+\boldsymbol{F}(\boldsymbol{U})_x=B(\boldsymbol{U})\boldsymbol{U}_x, \tag{4.1}$$

and follow the finite volume setting described in Section 2 to obtain its central-upwind semi-discretization:

$$\frac{d}{dt}\overline{\boldsymbol{U}}_j=-\frac{\boldsymbol{H}_{j+\frac{1}{2}}-\boldsymbol{H}_{j-\frac{1}{2}}}{\Delta x}+\overline{\boldsymbol{R}}_j, \tag{4.2}$$

where $\boldsymbol{H}_{j+\frac{1}{2}}$ are central-upwind numerical fluxes and $\overline{\boldsymbol{R}}_j$ are the computed cell averages of the nonconservative term on the RHS of equation (4.1).

The central-upwind numerical flux from [20] is

$$\boldsymbol{H}_{j+\frac{1}{2}}:=\frac{a^+_{j+\frac{1}{2}}\boldsymbol{F}(\boldsymbol{U}^-_{j+\frac{1}{2}})-a^-_{j+\frac{1}{2}}\boldsymbol{F}(\boldsymbol{U}^+_{j+\frac{1}{2}})}{a^+_{j+\frac{1}{2}}-a^-_{j+\frac{1}{2}}}+\frac{a^+_{j+\frac{1}{2}}a^-_{j+\frac{1}{2}}}{a^+_{j+\frac{1}{2}}-a^-_{j+\frac{1}{2}}}\left[\boldsymbol{U}^+_{j+\frac{1}{2}}-\boldsymbol{U}^-_{j+\frac{1}{2}}\right]. \tag{4.3}$$

Here, $\boldsymbol{U}^{\pm}_{j+\frac{1}{2}}$ are the right/left point values at $x=x_{j+\frac{1}{2}}$ of the piecewise linear reconstruction (2.3):

$$\boldsymbol{U}^+_{j+\frac{1}{2}}=\overline{\boldsymbol{U}}_{j+1}-\frac{\Delta x}{2}(\boldsymbol{U}_x)_{j+1},\quad \boldsymbol{U}^-_{j+\frac{1}{2}}=\overline{\boldsymbol{U}}_j+\frac{\Delta x}{2}(\boldsymbol{U}_x)_j.$$

Notice that now the numerical derivatives $\boldsymbol{U}_x$ are computed in a componentwise manner. The right- and left-sided local speeds $a^{\pm}_{j+\frac{1}{2}}$ in (4.3) are determined using the largest and smallest eigenvalues of the matrix

$$A(\boldsymbol{U})=\frac{\partial \boldsymbol{F}}{\partial \boldsymbol{U}}(\boldsymbol{U})-B(\boldsymbol{U})=\begin{pmatrix} \frac{3}{\sqrt{2}}u_2 & -1 & \frac{3}{2\sqrt{2}}u_1 & 0\\ -1+2\sqrt{2}\theta_2 & -\frac{1}{\sqrt{2}}u_2 & -\frac{1}{2\sqrt{2}}\theta_1 & \sqrt{2}u_1\\ 0 & 0 & 0 & -1\\ -\frac{1}{2\sqrt{2}}\theta_1 & \frac{1}{2\sqrt{2}}u_1 & -\frac{1}{4} & 0 \end{pmatrix},$$

which are to be calculated from the characteristic equation

$$\lambda^4+c_1\lambda^3+c_2\lambda^2+c_3\lambda+c_4=0, \tag{4.4}$$

with the coefficients

$$\begin{aligned} c_1&=-\sqrt{2}u_2,\\ c_2&=-\frac{1}{2}u_1^2-\frac{3}{2}u_2^2+2\sqrt{2}\theta_2-\frac{5}{4},\\ c_3&=-u_1\theta_1+\frac{3}{2\sqrt{2}}u_1^2u_2+\frac{1}{2\sqrt{2}}u_2,\\ c_4&=\frac{3}{2\sqrt{2}}u_1^2\theta_2-\frac{3}{8}u_1^2-\frac{1}{8}\theta_1^2+\frac{3}{8}u_2^2-\frac{1}{\sqrt{2}}\theta_2+\frac{1}{4}. \end{aligned}$$

Unfortunately, the analytic expressions for the roots of (4.4) are way too complicated and thus impractical. We therefore proceed along the lines of [23] and establish the desired bounds on the roots of (4.4) using the Lagrange theorem (see, e.g., [27]). According to this theorem, the largest nonnegative root is smaller than the sum of the largest and the second largest numbers in the set $\{\sqrt[j]{|c_j|}: j\in J_{\max}\}$, where $\{c_j: j\in J_{\max}\}$ is the set of the negative coefficients of (4.4). Similarly, the smallest nonpositive root of (4.4) is larger than the sum of the smallest and the second smallest numbers in the set $\{-\sqrt[j]{|d_j|}: j\in J_{\min}\}$, where $\{d_j: j\in J_{\min}\}$ is the set of negative coefficients of the polynomial

$$\lambda^4+d_1\lambda^3+d_2\lambda^2+d_3\lambda+d_4=0,\quad d_j=(-1)^j c_j,\quad \forall j.$$

We denote the obtained bounds by $\lambda_{\max}=\lambda_{\max}(u_1,\theta_1,u_2,\theta_2)$ and $\lambda_{\min}=\lambda_{\min}(u_1,\theta_1,u_2,\theta_2)$ and approximate the one-sided local speeds as

$$a^+_{j+\frac12}=\max_{\pm}\lambda_{\max}\Big((u_1)^{\pm}_{j+\frac12},(\theta_1)^{\pm}_{j+\frac12},(u_2)^{\pm}_{j+\frac12},(\theta_2)^{\pm}_{j+\frac12}\Big),$$
$$a^-_{j+\frac12}=\min_{\pm}\lambda_{\min}\Big((u_1)^{\pm}_{j+\frac12},(\theta_1)^{\pm}_{j+\frac12},(u_2)^{\pm}_{j+\frac12},(\theta_2)^{\pm}_{j+\frac12}\Big).$$

Remark 4.1. We would like to point out that if one considers a homogeneous system of hyperbolic conservation laws $\boldsymbol{U}_t+\boldsymbol{F}(\boldsymbol{U})_x=\boldsymbol{0}$, for which the one-sided local speeds $a^{\pm}_{j+\frac12}$ can be computed analytically, the first-order version of the described central-upwind scheme is exactly the semi-discrete version of the scheme from [14, 16, 17].

Finally, the non-conservative terms on the RHS of (4.1) are discretized as in [23] so that we obtain

$$\overline{\boldsymbol{R}}_j=B(\overline{\boldsymbol{U}}_j)\frac{\boldsymbol{U}^-_{j+\frac12}-\boldsymbol{U}^+_{j-\frac12}}{\Delta x}. \tag{4.5}$$

The central-upwind scheme described above is designed along the lines of [23], where it was applied to two-layer shallow water systems. A success of the central-upwind scheme for such systems hinged on the fact that the coefficients of the nonconservative terms were small in all practical applications. However, none of the three 2MSWE systems studied in this paper possess the same property. Therefore, a straightforward implementation of the central-upwind scheme to the 2MSWE may not be robust as we demonstrate in Examples 1 and 3 in Section 5 below.

We therefore present a robust version of the central-upwind scheme for nonconservative systems. It has been recently proposed in [11], where the concept of path-conservative central-upwind schemes has been introduced. In the next subsection, we develop a path-conservative central-upwind scheme for the 2MSWE and apply it to the systems (**I**), (**II**) and (**III**).

4.2 Path-conservative central-upwind scheme for the 2MSWE

Following the approach proposed in [11], we modify the central-upwind scheme (4.1), (4.2), (4.5) so that the jumps of the nonconservative terms at cell interfaces are taken into account. The path-conservative central-upwind scheme is then given by

$$\frac{d}{dt}\overline{\boldsymbol{U}}_j=-\frac{1}{\Delta x}\left(\boldsymbol{H}_{j+\frac{1}{2}}-\boldsymbol{H}_{j-\frac{1}{2}}+\frac{a^-_{j+\frac{1}{2}}}{a^+_{j+\frac{1}{2}}-a^-_{j+\frac{1}{2}}}\boldsymbol{B}_{\boldsymbol{\Psi},j+\frac{1}{2}}-\frac{a^+_{j-\frac{1}{2}}}{a^+_{j-\frac{1}{2}}-a^-_{j-\frac{1}{2}}}\boldsymbol{B}_{\boldsymbol{\Psi},j-\frac{1}{2}}\right)+\overline{\boldsymbol{R}}_j, \tag{4.6}$$

where for each one of the systems (**I**), (**II**) and (**III**), the fluxes $\boldsymbol{H}_{j+\frac{1}{2}}$ are computed from (4.3), the source $\overline{\boldsymbol{R}}_j$ is given by (4.5), and the terms that take into account possible jumps of the nonconservative terms across the cell interfaces (for details see [11]) are

$$\boldsymbol{B}_{\boldsymbol{\Psi},j+\frac{1}{2}}=\int_0^1 B(\boldsymbol{\Psi}_{j+\frac{1}{2}}(s))\frac{d\boldsymbol{\Psi}_{j+\frac{1}{2}}}{ds}ds, \tag{4.7}$$

in which $\boldsymbol{\Psi}_{j+\frac{1}{2}}(s)$ is a path

$$\boldsymbol{\Psi}_{j+\frac{1}{2}}(s)=\boldsymbol{\Psi}(s;\boldsymbol{U}^-_{j+\frac{1}{2}},\boldsymbol{U}^+_{j+\frac{1}{2}}):[0,1]\times\mathbb{R}^4\times\mathbb{R}^4\to\mathbb{R}^4,$$

such that

$$\boldsymbol{\Psi}(0;\boldsymbol{U}^-_{j+\frac{1}{2}},\boldsymbol{U}^+_{j+\frac{1}{2}})=\boldsymbol{U}^-_{j+\frac{1}{2}},\quad \boldsymbol{\Psi}(1;\boldsymbol{U}^-_{j+\frac{1}{2}},\boldsymbol{U}^+_{j+\frac{1}{2}})=\boldsymbol{U}^+_{j+\frac{1}{2}}.$$

In this paper, we use the simplest linear path

$$\boldsymbol{\Psi}_{j+\frac{1}{2}}(s)=\boldsymbol{U}^-_{j+\frac{1}{2}}+s(\boldsymbol{U}^+_{j+\frac{1}{2}}-\boldsymbol{U}^-_{j+\frac{1}{2}}),$$

which leads to the following expression for $\boldsymbol{B}_{\boldsymbol{\Psi},j+\frac{1}{2}}$ in (4.7):

$$\boldsymbol{B}_{\boldsymbol{\Psi},j+\frac{1}{2}}=\int_0^1 B\left(\boldsymbol{U}^-_{j+\frac{1}{2}}+s(\boldsymbol{U}^+_{j+\frac{1}{2}}-\boldsymbol{U}^-_{j+\frac{1}{2}})\right)(\boldsymbol{U}^+_{j+\frac{1}{2}}-\boldsymbol{U}^-_{j+\frac{1}{2}})ds=:\begin{pmatrix}\boldsymbol{B}^{(1)}_{\boldsymbol{\Psi},j+\frac{1}{2}}\\ \boldsymbol{B}^{(2)}_{\boldsymbol{\Psi},j+\frac{1}{2}}\\ \boldsymbol{B}^{(3)}_{\boldsymbol{\Psi},j+\frac{1}{2}}\\ \boldsymbol{B}^{(4)}_{\boldsymbol{\Psi},j+\frac{1}{2}}\end{pmatrix}.$$

The components of the vector $\boldsymbol{B}_{\boldsymbol{\Psi},j+\frac{1}{2}}$ can be computed for the systems (**I**), (**II**) and (**III**) explicitly and are given by:

System (I)

$$\begin{cases} \boldsymbol{B}^{(1)}_{\boldsymbol{\Psi},j+\frac{1}{2}} = -\dfrac{3}{2\sqrt{2}}[(u_2)^+_{j+\frac{1}{2}}+(u_2)^-_{j+\frac{1}{2}}][(u_1)^+_{j+\frac{1}{2}}-(u_1)^-_{j+\frac{1}{2}}] \\ \qquad\qquad -\dfrac{3}{4\sqrt{2}}[(u_1)^+_{j+\frac{1}{2}}+(u_1)^-_{j+\frac{1}{2}}][(u_2)^+_{j+\frac{1}{2}}-(u_2)^-_{j+\frac{1}{2}}], \\ \boldsymbol{B}^{(2)}_{\boldsymbol{\Psi},j+\frac{1}{2}} = -\sqrt{2}[(\theta_2)^+_{j+\frac{1}{2}}+(\theta_2)^-_{j+\frac{1}{2}}][(u_1)^+_{j+\frac{1}{2}}-(u_1)^-_{j+\frac{1}{2}}] \\ \qquad\qquad +\dfrac{1}{2\sqrt{2}}[(u_2)^+_{j+\frac{1}{2}}+(u_2)^-_{j+\frac{1}{2}}][(\theta_1)^+_{j+\frac{1}{2}}-(\theta_1)^-_{j+\frac{1}{2}}] \\ \qquad\qquad +\dfrac{1}{4\sqrt{2}}[(\theta_1)^+_{j+\frac{1}{2}}+(\theta_1)^-_{j+\frac{1}{2}}][(u_2)^+_{j+\frac{1}{2}}-(u_2)^-_{j+\frac{1}{2}}] \\ \qquad\qquad -\dfrac{1}{\sqrt{2}}[(u_1)^+_{j+\frac{1}{2}}+(u_1)^-_{j+\frac{1}{2}}][(\theta_2)^+_{j+\frac{1}{2}}-(\theta_2)^-_{j+\frac{1}{2}}], \\ \boldsymbol{B}^{(3)}_{\boldsymbol{\Psi},j+\frac{1}{2}} = 0, \\ \boldsymbol{B}^{(4)}_{\boldsymbol{\Psi},j+\frac{1}{2}} = \dfrac{1}{4\sqrt{2}}[(\theta_1)^+_{j+\frac{1}{2}}+(\theta_1)^-_{j+\frac{1}{2}}][(u_1)^+_{j+\frac{1}{2}}-(u_1)^-_{j+\frac{1}{2}}] \\ \qquad\qquad -\dfrac{1}{4\sqrt{2}}[(u_1)^+_{j+\frac{1}{2}}+(u_1)^-_{j+\frac{1}{2}}][(\theta_1)^+_{j+\frac{1}{2}}-(\theta_1)^-_{j+\frac{1}{2}}]; \end{cases}$$

System (II)

$$\begin{cases} \boldsymbol{B}^{(1)}_{\boldsymbol{\Psi},j+\frac{1}{2}} = \dfrac{3}{4\sqrt{2}}[(u_1)^+_{j+\frac{1}{2}}+(u_1)^-_{j+\frac{1}{2}}][(u_2)^+_{j+\frac{1}{2}}-(u_2)^-_{j+\frac{1}{2}}], \\ \boldsymbol{B}^{(2)}_{\boldsymbol{\Psi},j+\frac{1}{2}} = -\dfrac{1}{\sqrt{2}}[(\theta_2)^+_{j+\frac{1}{2}}+(\theta_2)^-_{j+\frac{1}{2}}][(u_1)^+_{j+\frac{1}{2}}-(u_1)^-_{j+\frac{1}{2}}] \\ \qquad\qquad -\dfrac{1}{4\sqrt{2}}[(\theta_1)^+_{j+\frac{1}{2}}+(\theta_1)^-_{j+\frac{1}{2}}][(u_2)^+_{j+\frac{1}{2}}-(u_2)^-_{j+\frac{1}{2}}], \\ \boldsymbol{B}^{(3)}_{\boldsymbol{\Psi},j+\frac{1}{2}} = 0, \\ \boldsymbol{B}^{(4)}_{\boldsymbol{\Psi},j+\frac{1}{2}} = \dfrac{1}{4\sqrt{2}}[(\theta_1)^+_{j+\frac{1}{2}}+(\theta_1)^-_{j+\frac{1}{2}}][(u_1)^+_{j+\frac{1}{2}}-(u_1)^-_{j+\frac{1}{2}}] \\ \qquad\qquad -\dfrac{1}{4\sqrt{2}}[(u_1)^+_{j+\frac{1}{2}}+(u_1)^-_{j+\frac{1}{2}}][(\theta_1)^+_{j+\frac{1}{2}}-(\theta_1)^-_{j+\frac{1}{2}}]; \end{cases}$$

System (III)

$$\begin{cases} \boldsymbol{B}^{(1)}_{\boldsymbol{\Psi},j+\frac{1}{2}} = \dfrac{3}{4\sqrt{2}}[(u_1)^+_{j+\frac{1}{2}} + (u_1)^-_{j+\frac{1}{2}}][(u_2)^+_{j+\frac{1}{2}} - (u_2)^-_{j+\frac{1}{2}}], \\ \boldsymbol{B}^{(2)}_{\boldsymbol{\Psi},j+\frac{1}{2}} = -\dfrac{1}{4\sqrt{2}}[(\theta_1)^+_{j+\frac{1}{2}} + (\theta_1)^-_{j+\frac{1}{2}}][(u_2)^+_{j+\frac{1}{2}} - (u_2)^-_{j+\frac{1}{2}}] \\ \qquad\qquad + \dfrac{1}{\sqrt{2}}[(u_1)^+_{j+\frac{1}{2}} + (u_1)^-_{j+\frac{1}{2}}][(\theta_2)^+_{j+\frac{1}{2}} - (\theta_2)^-_{j+\frac{1}{2}}], \\ \boldsymbol{B}^{(3)}_{\boldsymbol{\Psi},j+\frac{1}{2}} = 0, \\ \boldsymbol{B}^{(4)}_{\boldsymbol{\Psi},j+\frac{1}{2}} = \dfrac{1}{4\sqrt{2}}[(\theta_1)^+_{j+\frac{1}{2}} + (\theta_1)^-_{j+\frac{1}{2}}][(u_1)^+_{j+\frac{1}{2}} - (u_1)^-_{j+\frac{1}{2}}] \\ \qquad\qquad - \dfrac{1}{4\sqrt{2}}[(u_1)^+_{j+\frac{1}{2}} + (u_1)^-_{j+\frac{1}{2}}][(\theta_1)^+_{j+\frac{1}{2}} - (\theta_1)^-_{j+\frac{1}{2}}]. \end{cases}$$

Remark 4.2. A straightforward computation shows that the path-conservative central-upwind schemes for the systems (**I**), (**II**) and (**III**) are identical, that is, the RHS of (4.6) for all of these three systems is exactly the same provided the integral in (4.7) is evaluated exactly. The latter may be impossible if a more complicated, nonlinear path is selected.

Remark 4.3. Unfortunately, in nonconservative systems the speed of propagation of the discontinuities explicitly depends on the chosen family of paths, so that a good choice of paths is crucial to capture the physical meaningful weak solutions. A possible way to compute the correct paths could be based on the vanishing viscosity method: A parabolic regularization is considered with a small viscosity coefficient and the corresponding viscous profiles are then computed. If two states can be linked by an admissible discontinuity, the path connecting them should be the corresponding viscous profiles, for details see [33] and references therein. An important difference between conservative and nonconservative systems is that, in the nonconservative case, the jump conditions obtained from the vanishing viscosity method explicitly depend on the form of the viscous term. Nevertheless, the computation of viscous profiles for this problem is a very difficult task, and according to [10] the family of straight segments is a sensible choice, as their corresponding jump conditions are expected to give a third order approximation of the physically correct ones.

Moreover, according to [3,12], when the numerical viscosity of the method commutes with the Jacobian $\frac{\partial \boldsymbol{F}}{\partial \boldsymbol{U}}$, as it is the case for path-conservative central-upwind schemes, numerical solutions obtained by different paths for small/medium shocks do not differ too much, as the numerical shock curves associated with each scheme (or path) coincide up to third order in the size of the discontinuity.

5 Numerical examples

In this section, we perform a comparison study of the numerical methods presented in Section 3 and Section 4. We test the schemes on a number of numerical examples. The central-upwind scheme applied to the systems (**I**), (**II**) and (**III**) will be referred to as CUI, CUII and CUIII, respectively. A similar notation (PCCU) will be used for the path-conservative central-upwind scheme.

In all of the experiments, we use the minmod limiter (2.4) with $\gamma=1$ and the third-order strong stability preserving Runge-Kutta (SSP-RK) ODE solver (see, e.g. [15,34,35]) for time evolution. The size of the time steps is selected based on the theoretical CFL numbers, which are 0.5 for the CU and PCCU schemes and 1 for the upwind method.

We follow [36] and plot all of the numerical results in the dimensional units, that is, in all of the figures below, the velocities are multiplied by a factor of 50 and the temperatures are multiplied by a factor of $10\sqrt{2}$.

Example 1 – Dam Break Problem. We consider the 2MSWE subject to the following Riemann initial data:

$$\theta_1(x,0)=\begin{cases} -\dfrac{1}{\sqrt{2}}, & \text{if } x<0,\\ 0, & \text{if } x>0,\end{cases} \qquad \theta_2(x,0)\equiv u_1(x,0)\equiv u_2(x,0)\equiv 0.$$

We take a uniform grid with $\Delta x=0.5$ and compute the solution at time $t=360$. This example is a slightly modified version of the dam break problem considered in [36, §5.4].

We first solve the systems (**I**), (**II**) and (**III**) using the CUI, CUII, CUIII schemes and plot the results in Fig. 1. As one can see, the solutions computed by these schemes are different, which demonstrates that the obtained numerical results clearly depend on the way nonconservative terms are treated. Next, in Figs. 2-4, we compare the results obtained by the three central-upwind schemes with those computed by the PCCU scheme. Finally, we apply the splitting method from Section 3 to this initial-value problem and show in Fig. 5 a good agreement between solutions obtained by the PCCU scheme and the splitting method.

Example 2 — Waves Generated by Thermal Forcing. In this example, also considered in [36], we solve a more general 2MSWE

$$\boldsymbol{U}_t+\boldsymbol{F}(\boldsymbol{U})_x=\boldsymbol{R}(\boldsymbol{U},\boldsymbol{U}_x)+\boldsymbol{S}(x)$$

subject to the constant initial data

$$u_1(x,0)\equiv\frac{1}{\sqrt{2}},\quad u_2(x,0)\equiv-\frac{1}{\sqrt{2}},\quad \theta_1(x,0)\equiv\theta_2(x,0)\equiv 0.$$

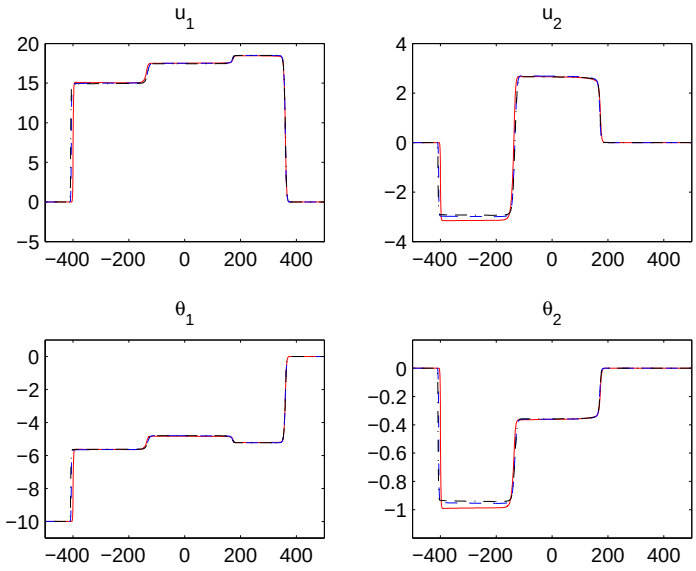

Figure 1: Example 1: Comparison of CUI (solid line), CUII (dashed line) and CUIII (dash-dot line) results.

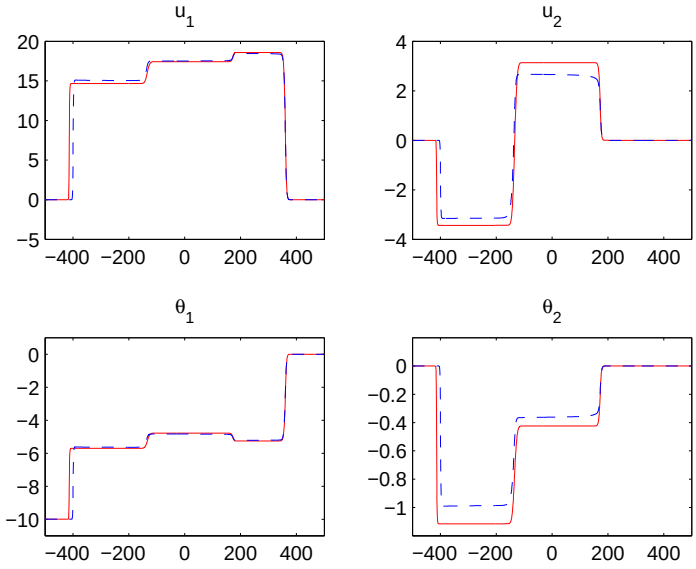

Figure 2: Example 1: PCCU (solid line) vs. CUI (dashed line) results.

In this model, a thermal source S is taken into account and given by

$$\boldsymbol{S}(x) = (0, S_{\theta_1}, 0, S_{\theta_2})^T,$$

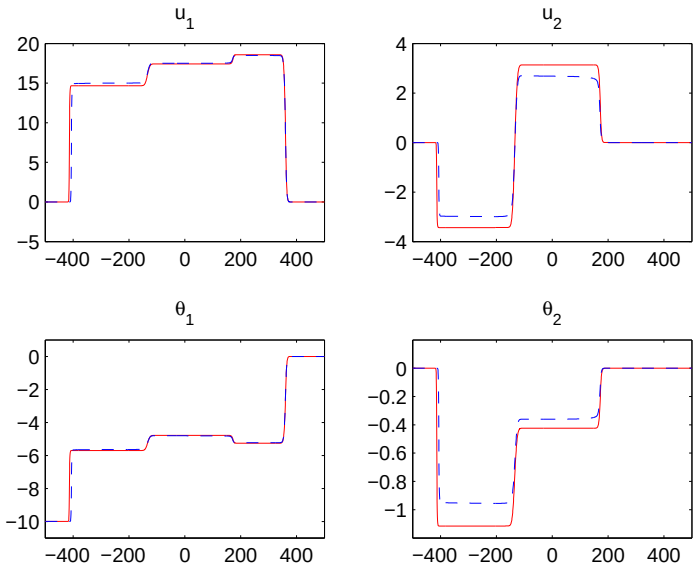

Figure 3: Example 1: PCCU (solid line) vs. CUII (dashed line) results.

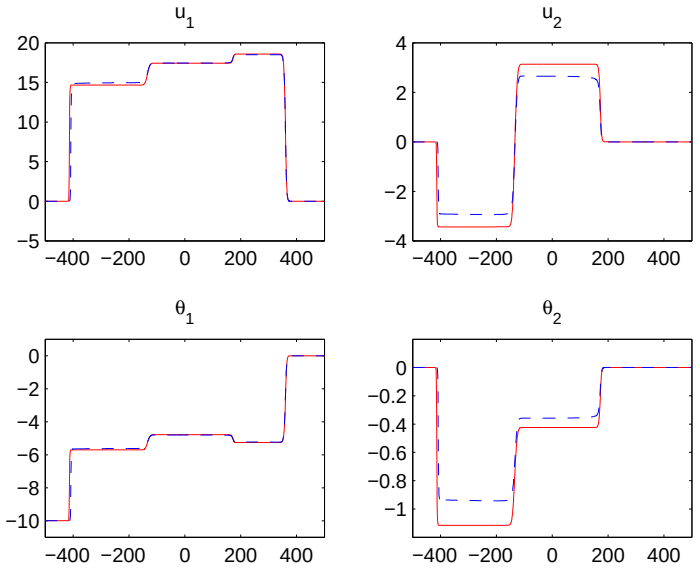

Figure 4: Example 1: PCCU (solid line) vs. CUIII (dashed line) results.

where

$$S_{\theta_1} = ae^{-\frac{(x-x_0)^2}{2\sigma^2}}, \quad S_{\theta_2} = -\frac{1}{4}S_{\theta_1}. \tag{5.1}$$

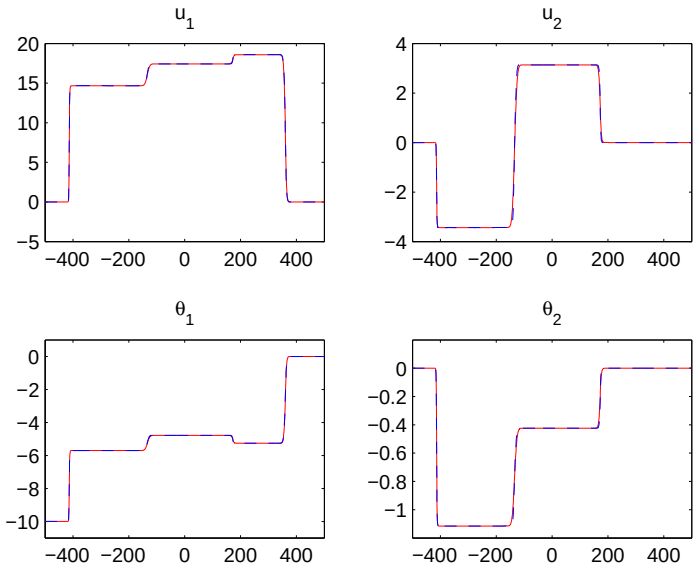

Figure 5: Example 1: PCCU (solid line) vs. Upwind Splitting (dashed line) results.

The heating is centered at $x_0=1000$, the standard deviation in (5.1) is $\sigma=20$, and the amplitude is $a=\sqrt{2}/450$.

We introduce a uniform grid with $\Delta x=1$ and compute the solution at time $t=720$, using all the studied schemes, which in the presence of the thermal source term can be written as (compare with (2.2)):

$$\frac{d}{dt}\overline{\boldsymbol{U}}_j=-\frac{\boldsymbol{H}_{j+\frac{1}{2}}-\boldsymbol{H}_{j-\frac{1}{2}}}{\Delta x}+\overline{\boldsymbol{R}}_j+\overline{\boldsymbol{S}}_j,\quad \overline{\boldsymbol{S}}_j\approx\frac{1}{\Delta x}\int_{I_j}\boldsymbol{S}(x)dx.$$

The thermal source is discretized using the midpoint rule, that is, we take $\overline{\boldsymbol{S}}_j=S(x_j)$.

In this example, all four central-upwind schemes (CUI, CUII, CUIII, PCCU) and the splitting method produce quite similar results, which are plotted in Figs. 6-9.

Example 3 – Riemann Problem I. We consider an initial-value problem, which is similar to the one studied in Example 1, but has a more complicated Riemann initial data:

$$(u_1(x,0),\theta_1(x,0),u_2(x,0),\theta_2(x,0))=\begin{cases}(0.5,-0.7,-1,-0.5), & \text{if } x<0,\\ (-0.8,0.2,1.5,0.2), & \text{if } x>0.\end{cases}$$

We compute the solution at time t=90 using a uniform grid of size Δx=0.5. In Figs. 11-13, we again compare the CUI, CUII and CUIII solutions with the PCCU one. As one can see, the differences in the obtained results are quite large. Even though the CUII and CUIII

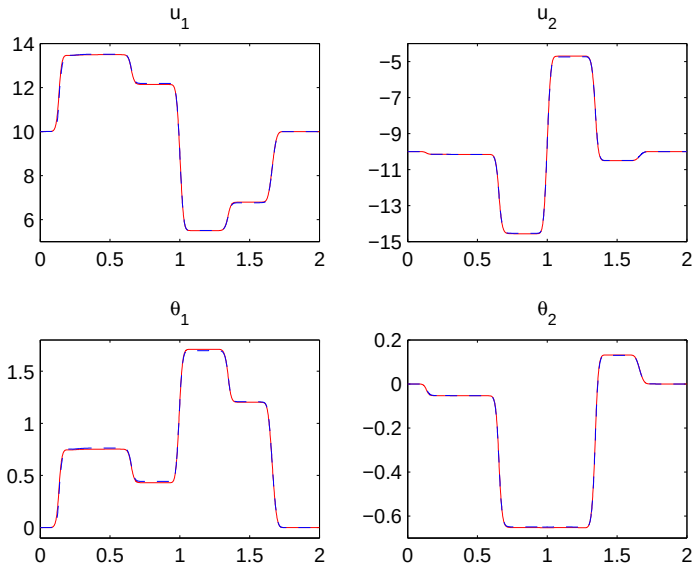

Figure 6: Example 2: PCCU (solid line) vs. CUI (dashed line) results.

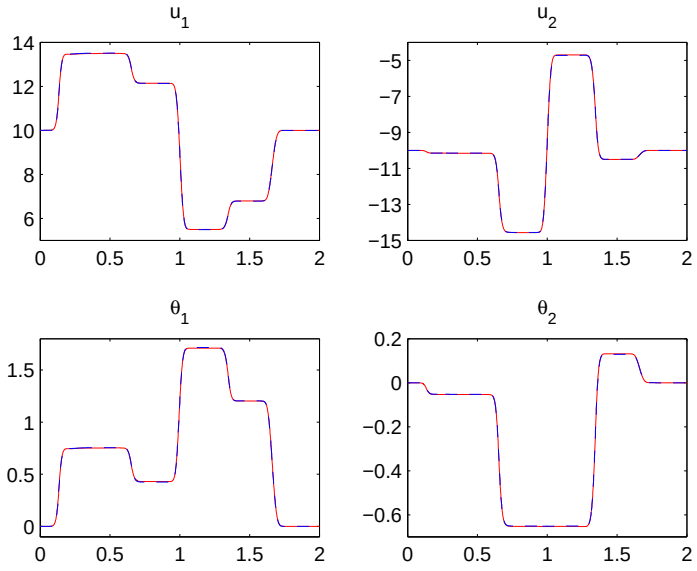

Figure 7: Example 2: PCCU (solid line) vs. CUII (dashed line) results.

results are close (see Fig. 10), they are not able to accurately represent the jumps at the cell interfaces which affect the resolution of the nonconservative terms.

On the other hand, the upwind splitting method produces results, which are similar

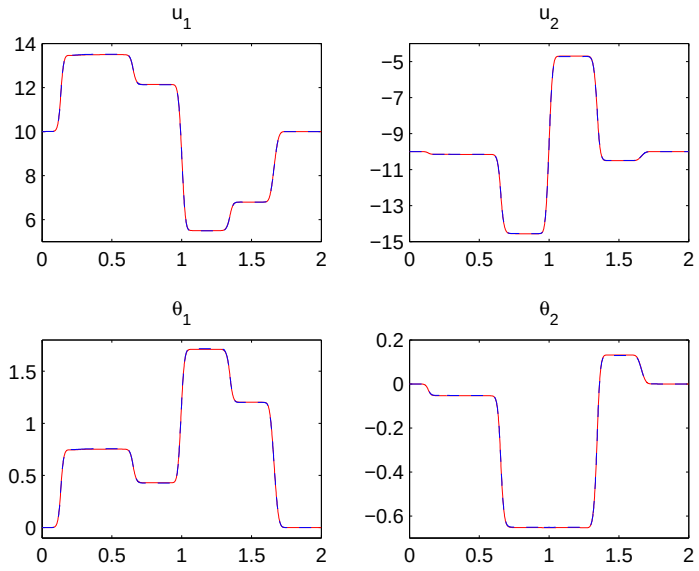

Figure 8: Example 2: PCCU (solid line) vs. CUIII (dashed line) results.

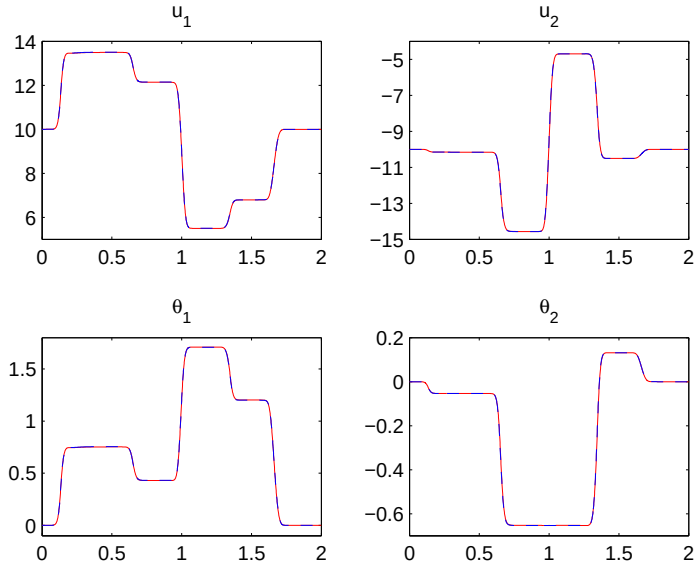

Figure 9: Example 2: PCCU (solid line) vs. Upwind Splitting (dashed line) results.

to the PCCU ones. However, there is still some discrepancy between the computed solutions (see Fig. 14). We further study the behavior of the PCCU scheme and upwind splitting method by performing a mesh refinement study. The PCCU results seem to

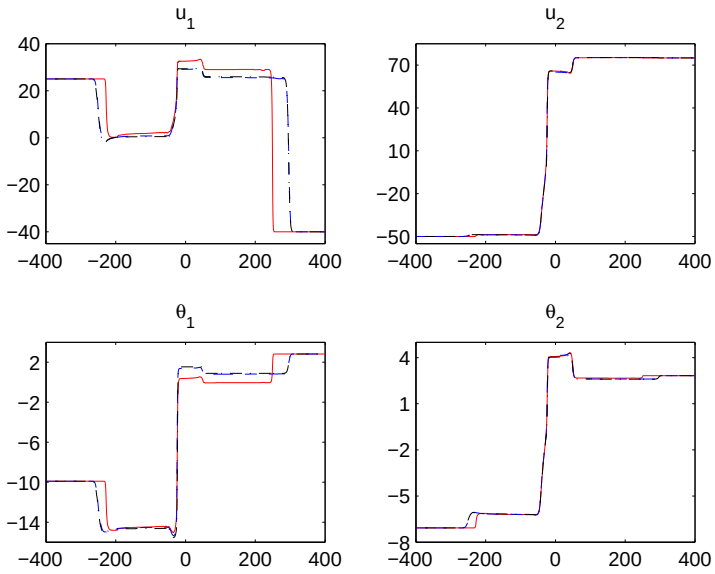

Figure 10: Example 3: Comparison of CUI (solid line), CUII (dashed line) and CUIII (dash-dot line) results.

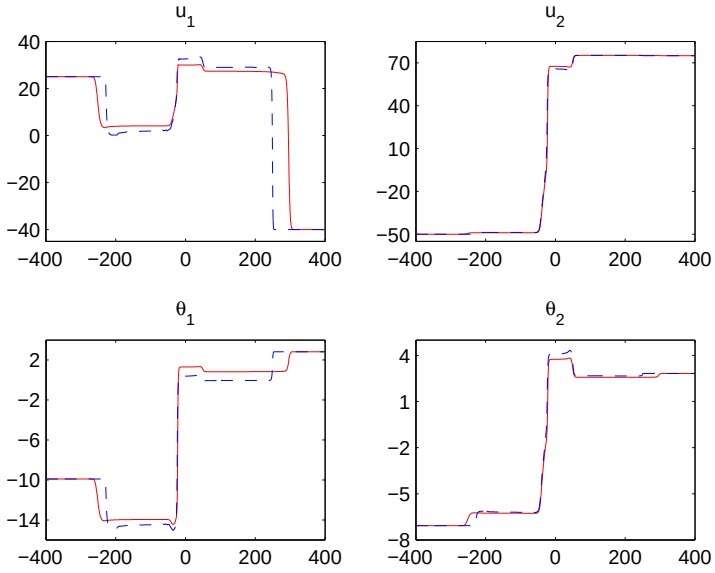

Figure 11: Example 3: PCCU (solid line) vs. CUI (dashed line) results.

clearly converge (see Figs. 15, 16), while the splitting solution develops small structural oscillations (see Fig. 17), which are especially pronounced when we zoom at the areas of interest in Fig. 18.

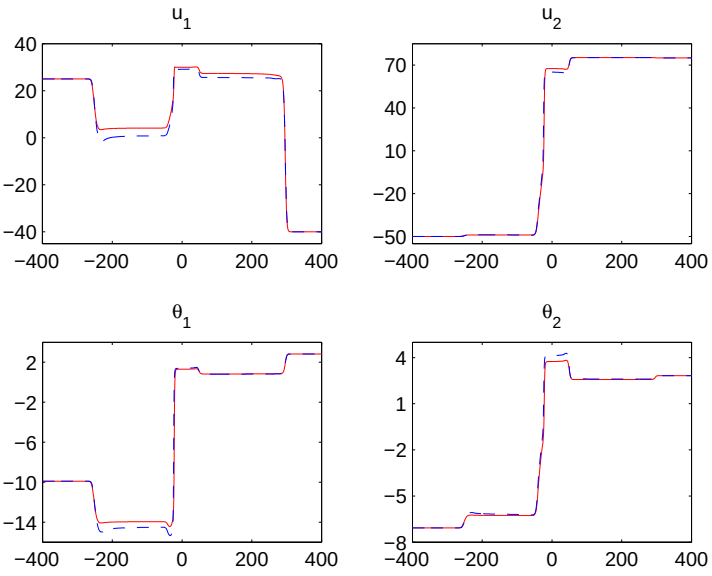

Figure 12: Example 3: PCCU (solid line) vs. CUII (dashed line) results.

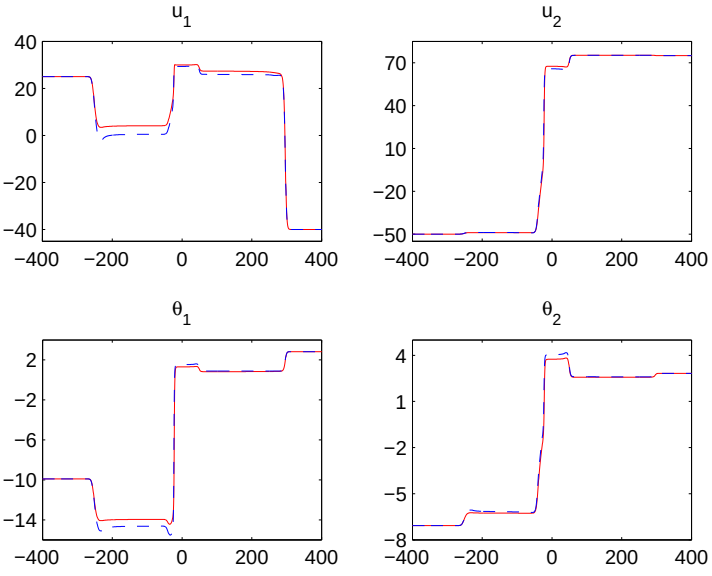

Figure 13: Example 3: PCCU (solid line) vs. CUIII (dashed line) results.

This example suggests that among the studied methods, the PCCU scheme provides the most robust and accurate tool for the 2MSWE.

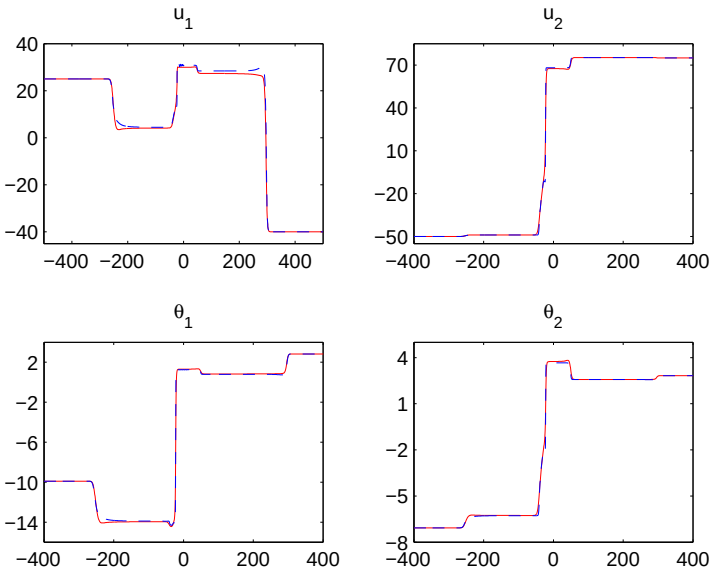

Figure 14: Example 3: PCCU (solid line) vs. Upwind Splitting (dashed line) results.

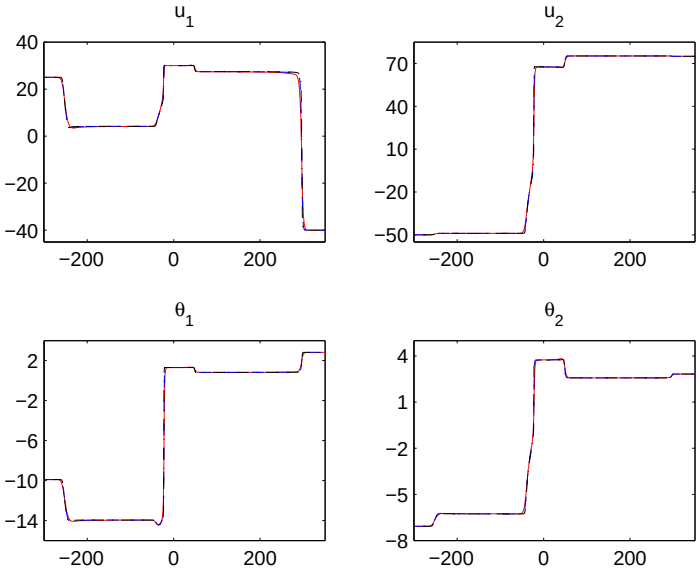

Figure 15: Example 3: PCCU results on the three different grids with $\Delta x = 0.5$ (solid line), 0.25 (dashed line) and 0.125 (dash-dot line).

Example 4 – Riemann Problem II. Finally, we consider another Riemann problem with the following initial data:

$$(u_1(x,0),\theta_1(x,0),u_2(x,0),\theta_2(x,0)) = \begin{cases} (1,0.9,-0.9,0.4), & \text{if } x<0, \\ (0.7,-0.6,-0.4,0.45), & \text{if } x>0. \end{cases} \tag{5.2}$$

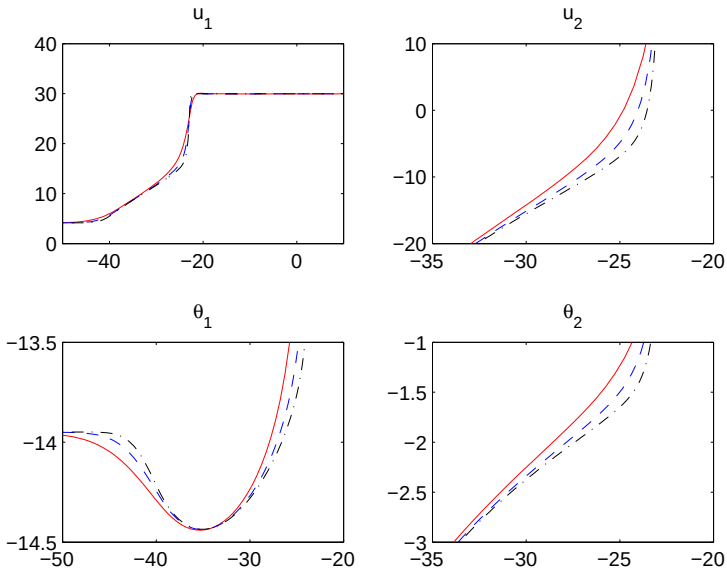

Figure 16: Example 3: The same as Fig. 15, but zoomed at the areas of interest.

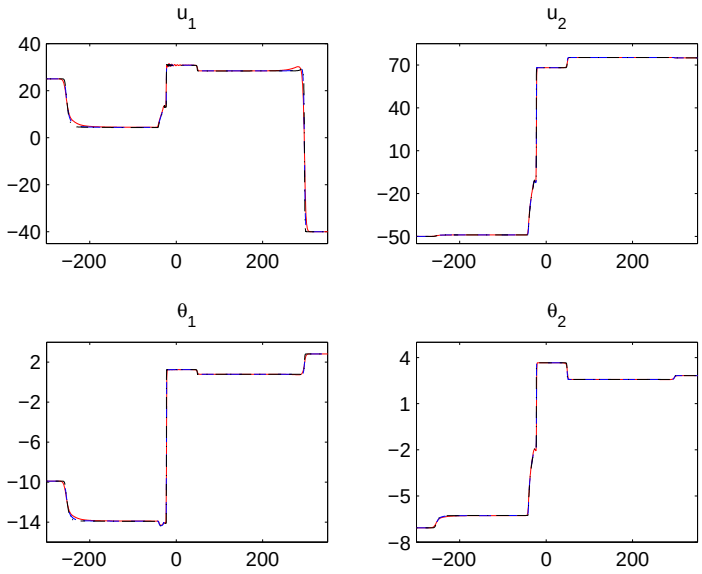

Figure 17: Example 3: Upwind Splitting results on the three different grids with $\Delta x = 0.5$ (solid line), 0.25 (dashed line) and 0.125 (dash-dot line).

We compute the solution at time t=180 using a uniform grid of size Δx=0.5. In Fig. 19, we plot the CUI, CUII and CUIII solutions, which are very different from each other. Then

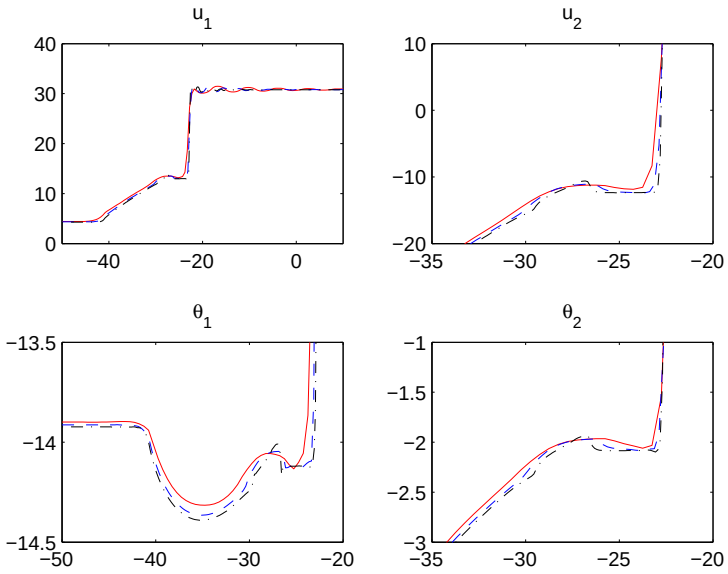

Figure 18: Example 3: The same as Fig. 17, but zoomed at the areas of interest.

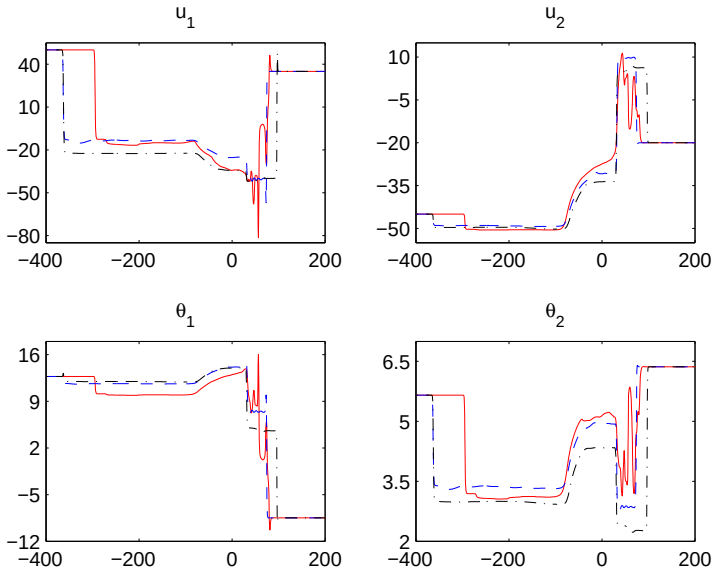

Figure 19: Example 4: Comparison of CUI (solid line), CUII (dashed line) and CUIII (dash-dot line) results.

in Figs. 20-22, we compare the above three results with the PCCU one. As one can see, the CU scheme cannot accurately reproduce the PCCU results no matter which system (**I**), (**II**) or (**III**) is solved.

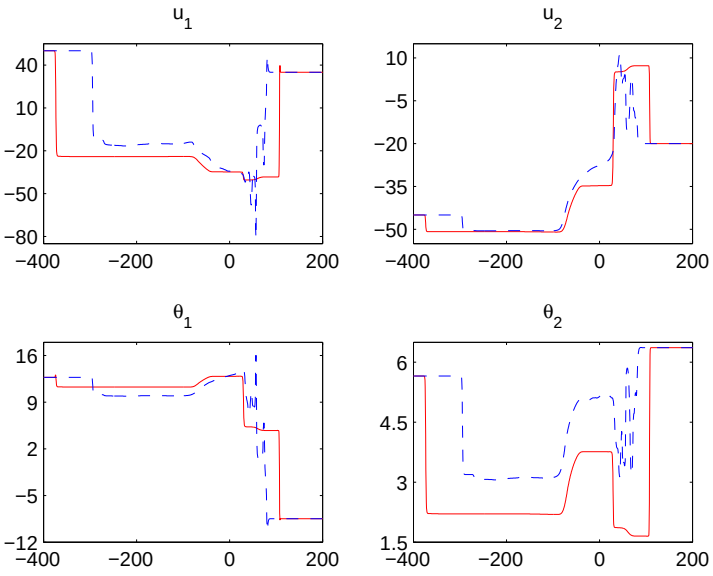

Figure 20: Example 4: PCCU (solid line) vs. CUI (dashed line) results.

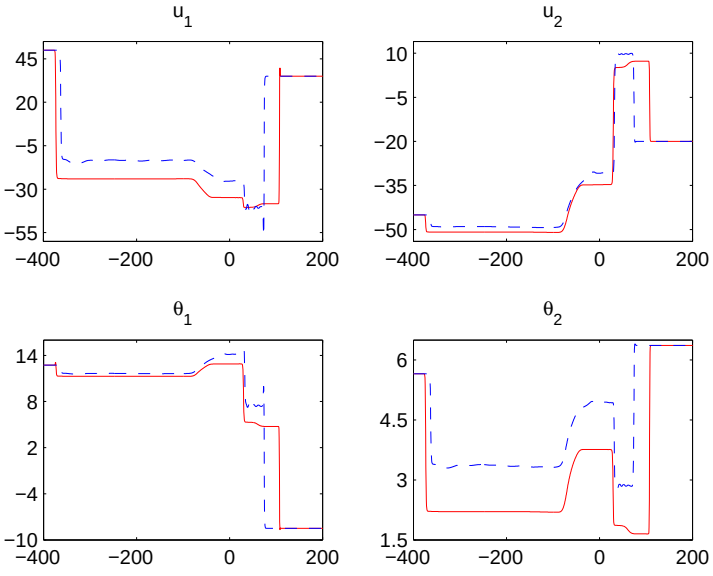

Figure 21: Example 4: PCCU (solid line) vs. CUII (dashed line) results.

Next, we find out that the upwind splitting method from Section 3 does not work since in this problem, the solution is close to the nonhyperbolic regime and the diagonalization described in Section 3.1 fails due to the appearance of negative values under

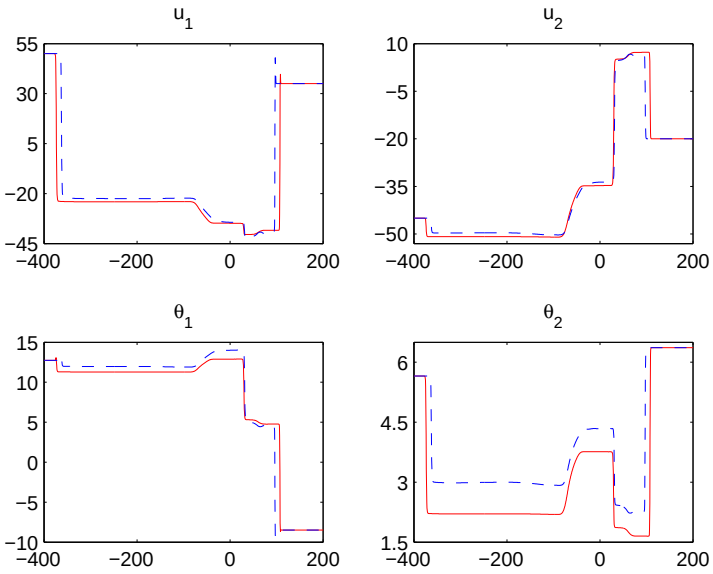

Figure 22: Example 4: PCCU (solid line) vs. CUIII (dashed line) results.

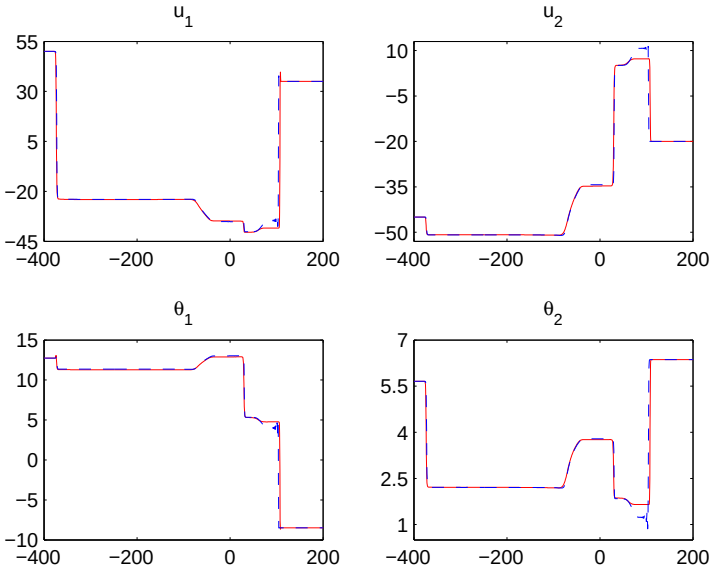

Figure 23: Example 4: PCCU (solid line) vs. Central-Upwind Splitting (dashed line) results.

the square roots. We therefore solve the split systems (1.5a), (1.6) and (1.5b), (1.7) by the second-order central-upwind scheme similar to the one presented in Section 4.1. The obtained results are shown in Fig. 23 together with the PCCU ones. As one can see, the

use of the central-upwind splitting method leads to significant errors in the area near the right-going shock wave.

To understand the reason the splitting methods do not work well in this example, we compare the eigenvalues of the 2MSWE obtained by numerically solving the characteristic equation (4.4) with the eigenvalues of the systems (1.5a), (1.6) and (1.5b), (1.7), see Table 1. As one can see, the eigenvalues of the full system and split systems are very different, which explains the discrepancy in the obtained numerical results.

Table 1: The eigenvalues for the left and right states in (5.2).

Initial data	Eigenvalues of the 2MSWE	Eigenvalues of the systems (1.5a), (1.6) and (1.5b), (1.7)
$u_1=1,\theta_1=0.9$ $u_2=-0.9,\theta_2=0.4$	-1.3459, -1.3269 0.0938, 1.3062	-1.8565, -0.5000 0.5000, 0.5837
$u_1=0.7,\theta_1=-0.6$ $u_2=-0.4,\theta_2=0.45$	-1.0647,0.0856 0.1118,0.3017	-0.5001,-0.5000 -0.0656,0.5000

6 Conclusion

In this paper, we have introduced three second-order numerical methods for the 2MSWE, which admit several different forms. The 2MSWE were derived in [36] in form of the system (**I**). The system (**II**) was proposed in [36] as a better form for solving the 2MSWE numerically. In this paper, we have rewritten the 2MSWE in form of the system (**III**), which is suitable for designing an operator splitting method, which has been implemented in conjunction with the Roe-type upwinding. The presented operator splitting method has performed well in most of the numerical experiments. However, in some cases it develops structural oscillations, which can be attributed to the splitting error. We have also applied the Riemann-problem-solver-free central-upwind scheme to all of the three systems and showed that the results depend on the way the 2MSWE system is written. The latter illustrates the fact that the presence of nonconservative terms makes it difficult to design a robust numerical method. We therefore modify the central-upwind scheme and derive its path-conservative version, which produces identical results for the aforementioned three different versions of the 2MSWE. Moreover, the conducted mesh refinement study clearly demonstrates a super performance of the presented path-conservative central-upwind scheme.

Acknowledgments

The work of M. J. Castro was supported in part by Spanish Government and FEDER through the Research project MTM2012-38383-C02-01, and by the Andalusian Government through the project P11-FQM8179. The work of A. Chertock was supported in part

by the NSF Grant DMS-1216974 and the ONR Grant N00014-12-1-0832. The work of A. Kurganov was supported in part by the NSF Grant DMS-1216957 and the ONR Grant N00014-12-1-0833. The work of Y. Cheng was supported in part by the summer research stipend granted by the Mathematics Department at Tulane University. Part of this research was conducted during the Summer of 2012, when Y. Cheng, A. Chertock and A. Kurganov visited the Institute of Natural Sciences at the Shanghai Jiao Tong University, China. The authors would like to thank the faculty, staff and especially the Institute co-director Prof. Shi Jin for their support and hospitality.

References

[1] R. Abgrall and S. Karni, Two-layer shallow water system: a relaxation approach, SIAM J. Sci. Comput. 31 (2009), no. 3, 1603–1627.
[2] R. Abgrall and S. Karni, A comment on the computation of non-conservative products, J. Comput. Phys. 229 (2010), no. 8, 2759–2763.
[3] F. Alouges and B. Merlet, Approximate shock curves for non-conservative hyperbolic systems in one space dimension, J. Hyperbolic Differ. Equ. 1 (2004), no. 4, 769–788.
[4] F. Bouchut and T. Morales de Luna, An entropy satisfying scheme for two-layer shallow water equations with uncoupled treatment, M2AN Math. Model. Numer. Anal. 42 (2008), 683–698.
[5] F. Bouchut and V. Zeitlin, A robust well-balanced scheme for multi-layer shallow water equations, Discrete Contin. Dyn. Syst. Ser. B 13 (2010), no. 4, 739–758.
[6] M. Castro, J. Macías, and C. Parés, A Q-scheme for a class of systems of coupled conservation laws with source term. Application to a two-layer 1-D shallow water system, M2AN Math. Model. Numer. Anal. 35 (2001), no. 1, 107–127.
[7] M.J. Castro, P.G. LeFloch, M.L. Muñoz-Ruiz, and C. Parés, Why many theories of shock waves are necessary: convergence error in formally path-consistent schemes, J. Comput. Phys. 227 (2008), no. 17, 8107–8129.
[8] M.J. Castro, C. Parés, G. Puppo, and G. Russo, Central schemes for nonconservative hyperbolic systems, SIAM J. Sci. Comput. 34 (2012), no. 5, B523–B558.
[9] M. J. Castro Díaz, T. Chacón Rebollo, E. D. Fernández-Nieto, and C. Pares, On well-balanced finite volume methods for nonconservative nonhomogeneous hyperbolic systems, SIAM J. Sci. Comput. 29 (2007), no. 3, 1093–1126.
[10] M.J. Castro Díaz, E.D. Fernández-Nieto, T. Morales de Luna, G. Narbona-Reina, and C. Parés, A HLLC scheme for nonconservative hyperbolic problems. Application to turbidity currents with sediment transport, M2AN Math. Model. Numer. Anal. 47 (2013), no. 01, 1–32.
[11] M.J. Castro Díaz, A. Kurganov, and T. Morales de Luna, Path-conservative central-upwind schemes for nonconservative hyperbolic systems, In preparation.
[12] N. Chalmers and E. Lorin, On the numerical approximation of one-dimensional nonconservative hyperbolic systems, J. Comput. Science 4 (2013), 111–124.
[13] G. Dal Maso, P.G. Lefloch, and F. Murat, Definition and weak stability of nonconservative products, J. Math. Pures Appl. (9) 74 (1995), no. 6, 483–548.
[14] B. Einfeld, On Godunov-type methods for gas dynamics, SIAM J. Numer. Anal. 25 (1988), 294–318.

[15] S. Gottlieb, C.-W. Shu, and E. Tadmor, Strong stability-preserving high-order time discretization methods, SIAM Rev. 43 (2001), 89–112.
[16] A. Harten, P. Lax, and B. van Leer, On upstream differencing and Godunov-type schemes for hyperbolic conservation laws, SIAM Rev. 25 (1983), 35–61.
[17] A. Harten and P.D. Lax, A random choice finite difference scheme for hyperbolic conservation laws, SIAM J. Numer. Anal. 18 (1981), no. 2, 289–315.
[18] A. Kurganov and D. Levy, Central-upwind schemes for the saint-venant system, M2AN Math. Model. Numer. Anal. 36 (2002), 397–425.
[19] A. Kurganov and C.-T. Lin, On the reduction of numerical dissipation in central-upwind schemes, Commun. Comput. Phys. 2 (2007), 141–163.
[20] A. Kurganov, S. Noelle, and G. Petrova, Semi-discrete central-upwind scheme for hyperbolic conservation laws and Hamilton-Jacobi equations, SIAM J. Sci. Comput. 23 (2001), 707–740.
[21] A. Kurganov and G. Petrova, A second-order well-balanced positivity preserving central-upwind scheme for the saint-venant system, Commun. Math. Sci. 5 (2007), 133–160.
[22] A. Kurganov and G. Petrova, A central-upwind scheme for nonlinear water waves generated by submarine landslides, Hyperbolic problems: theory, numerics, applications (Lyon 2006) (S. Benzoni-Gavage and D. Serre, eds.), Springer, 2008, pp. 635–642.
[23] A. Kurganov and G. Petrova, Central-upwind schemes for two-layer shallow equations, SIAM J. Sci. Comput. 31 (2009), 1742–1773.
[24] A. Kurganov and E. Tadmor, New high resolution central schemes for nonlinear conservation laws and convection-diffusion equations, J. Comput. Phys. 160 (2000), 241–282.
[25] K.-A. Lie and S. Noelle, On the artificial compression method for second-order nonoscillatory central difference schemes for systems of conservation laws, SIAM J. Sci. Comput. 24 (2003), no. 4, 1157–1174.
[26] J. Macías, C. Pares, and M.J. Castro, Improvement and generalization of a finite element shallow-water solver to multi-layer systems, Internat. J. Numer. Methods Fluids 31 (1999), no. 7, 1037–1059.
[27] M. Mignotte and D. Stefanescu, On an estimation of polynomial roots by lagrange, Tech. Report 025/2002, pp. 1–17, IRMA Strasbourg, `http://hal.archives-ouvertes.fr/hal-00129675/en/`, 2002.
[28] M.L. Muñoz-Ruiz and C. Parés, Godunov method for nonconservative hyperbolic systems, M2AN Math. Model. Numer. Anal. 41 (2007), no. 1, 169–185.
[29] M.L. Muñoz-Ruiz and C. Parés, On the convergence and well-balanced property of path-conservative numerical schemes for systems of balance laws, J. Sci. Comput. 48 (2011), no. 1-3, 274–295.
[30] H. Nessyahu and E. Tadmor, Nonoscillatory central differencing for hyperbolic conservation laws, J. Comput. Phys. 87 (1990), no. 2, 408–463.
[31] C. Parés, Numerical methods for nonconservative hyperbolic systems: a theoretical framework, SIAM J. Numer. Anal. 44 (2006), no. 1, 300–321.
[32] C. Parés, Path-conservative numerical methods for nonconservative hyperbolic systems, Numerical methods for balance laws, Quad. Mat., vol. 24, Dept. Math., Seconda Univ. Napoli, Caserta, 2009, pp. 67–121.
[33] C. Parés and M.L. Muñoz-Ruiz, On some difficulties of the numerical approximation of nonconservative hyperbolic systems, Bol. Soc. Esp. Mat. Apl. S$\vec{e}$MA (2009), no. 47, 23–52.
[34] C.-W. Shu, Total-variation-diminishing time discretizations, SIAM J. Sci. Comput. 6 (1988), 1073–1084.
[35] C.-W. Shu and S. Osher, Efficient implementation of essentially non-oscillatory shock-

capturing schemes, J. Comput. Phys. 77 (1988), 439–471.
[36] S. Stechmann, A. Majda, and B. Khouider, Nonlinear dynamics of hydrostatic internal gravity waves, Theor. Comput. Fluid Dyn. 22 (2008), 407–432.
[37] G. Strang, On the construction and comparison of difference schemes, SIAM J. Numer. Anal. 5 (1968), 506–517.
[38] P.K. Sweby, High resolution schemes using flux limiters for hyperbolic conservation laws, SIAM J. Numer. Anal. 21 (1984), no. 5, 995–1011.
[39] G.K. Vallis, Atmospheric and oceanic fluid dynamics: fundamentals and large-scale circulation, Cambridge University Press, 2006.
[40] B. van Leer, Towards the ultimate conservative difference scheme. V. A second-order sequel to Godunov's method, J. Comput. Phys. 32 (1979), no. 1, 101–136.